1967ApJ...147..471M

GALACTIC H II REGIONS. I. OBSERVATIONS OF THEIR CONTINUUM RADIATION AT THE FREQUENCY 5 GHz

P. G. MEZGER AND A. P. HENDERSON*
National Radio Astronomy Observatory,† Green Bank, West Virginia
Received June 10, 1966; revised August 8, 1966

ABSTRACT

The continuum radiation of thirteen galactic radio sources was mapped at a wavelength $\lambda = 6$ cm. The NRAO 140-foot telescope was used for this survey; the half-power beam widths are 6.'45 (*E* plane) and 6.'3 (*H* plane), the beam efficiency is 0 81 and the aperture efficiency is 0 525 at this wavelength.

Most of the investigated sources are resolved into two or more components The peak temperatures and the half-power widths of these components are computed by fitting Gaussian curves through the measured cross-sections The flux densities of the bright emission centers and the integrated flux density of the total radio source (after separation from the unresolved background radiation) are given. The positions of the emission centers are given with an accuracy between $\pm 1'$ and $\pm 3'$

The observation of the hydrogen 109α recombination line of these sources allows an unambiguous identification of H II regions as well as an estimate of their distances and electron temperatures. The measured flux densities, together with these latter parameters, yield the total mass of ionized hydrogen, the average electron densities, and the maximum emission measures for the bright emission centers of the investigated H II regions.

I. INTRODUCTION

In the course of our survey of hydrogen 109α recombination-line radiation at 5009 MHz (Mezger and Höglund; referred to hereinafter as "Paper II"), it was found necessary to supplement the line observations with a continuum survey. This continuum survey was to provide us with the following information: (i) a detailed brightness temperature distribution of the sources (this is especially important where sources previously considered to be single sources have now been resolved in two or more components); (ii) the angular size; (iii) the positions; (iv) the flux densities and maximum antenna (and brightness) temperatures of the resolved sources.

The hydrogen-recombination-line survey provided us with both the approximate distance and the electron temperature of the investigated H II regions (Paper II). Combining the results of both the line and the continuum survey we derive in this paper: (v) the linear dimensions; (vi) the average electron density; (vii) an upper limit for the total mass of ionized hydrogen; (viii) the distance (*z*-coordinate) from the galactic plane of the investigated H II regions.

II. RADIO TELESCOPE AND RADIOMETER

The observations were made during July and August, 1965, with the recently completed NRAO 140-foot telescope.

The radiometer, a superheterodyne receiver which was preceded by a parametric amplifier, could be operated either as a frequency-switched line receiver or as a continuum radiometer. In the latter case the radiometer input was switched between the feed and a sky horn. This sky horn was pointed in a direction opposite to the reflector and tilted away from the electrical axis of the telescope about 15° toward north. A filter between mixer and parametric amplifier suppressed reception at the image frequency. The system noise temperature was about 450° K with the telescope pointed toward the zenith. The crystal-controlled local oscillator was tuned to a frequency which resulted

* University of Maryland, College Park, Maryland.

† The National Radio Astronomy Observatory is operated by Associated Universities, Inc., under contract with the National Science Foundation.

© American Astronomical Society • Provided by the NASA Astrophysics Data System

1967ApJ...147..471M

in a center frequency of 5009 MHz of the 8 MHz wide reception band. The continuum observations were recorded with an analogue recorder. Time and position marks could be entered manually into the records. Two calibration marks, corresponding to antenna temperatures of 101.5° and 7° K, were derived from an argon-noise tube and were used as substandards throughout the observations. The large calibration mark was calibrated with a cooled load as an absolute calibration standard.

The 140-foot telescope is polar mounted; its construction and the results of preliminary tests at wavelengths between 11 and 1.95 cm are described elsewhere (Small 1965; Baars and Mezger 1966). The half-power beam width ("HPBW") of the telescope was derived from declination scans through Cygnus A; values of $\theta_E = 6'.45$ and $\theta_H = 6'.3$ for the E and H plane were obtained. A source width of 1′ was adopted for this calculation. Aperture efficiency, η_A, and beam efficiency, η_B, were calibrated with sources whose diameters are of the order of the antenna HPBW. The observed antenna temperature distribution was integrated, and the relation

$$\eta_B = \frac{2k}{\lambda^2 S_\nu} \int_{\text{source}} T_A d\Omega , \qquad k = 1.38 \times 10^{-23} \text{W s/°K} , \tag{1}$$

was used to determine the beam efficiency. Four calibration sources were used whose flux density has been recently reanalyzed (Baars, Mezger, and Wendker 1965*b*).

TABLE 1

ADOPTED FLUX DENSITIES FOR TELESCOPE CALIBRATION

Source	Adopted Flux Density 1965 5 (W m^{-2} Hz^{-1}) $\times 10^{26}$	Beam Efficiency
Cassiopeia A	859	0.80
Cygnus A	375	79
Taurus A	654	.84
Virgo A	75	0 81

The adopted flux densities and the values of the beam efficiency derived from the integrated contour maps are given in Table 1. The relation

$$\eta_A = \frac{4\lambda^2}{\pi \Omega_m d^2} \eta_B , \tag{2}$$

with $d = 42.7$ m the diameter of the telescope aperture and $\Omega_m = 1.133\ \theta_E \theta_H$ the main-beam solid angle, has been used to compute the aperture efficiency. We derived in this way the following values:

beam efficiency, $\eta_B = 0.81 \pm 0.02$; aperture efficiency, $\eta_A = 0.525 \pm 0.03$.

The quoted errors are estimated. We refer to Baars and Mezger (1966) for a discussion of the changes of the telescope characteristics with telescope position. The attenuation of the first sidelobes was more than 24 db.

III. OBSERVATIONS AND DATA REDUCTION

At $\lambda = 6$ cm the influence of sky-noise fluctuations on radio astronomical observations becomes a serious problem; these fluctuations are apparently caused by fluctua-

© American Astronomical Society • Provided by the NASA Astrophysics Data System

1967ApJ...147..471M

tions of the water-vapor density in the atmosphere within the main beam of the antenna. Mapping of extended sources was therefore performed only during "good" to "fair" observing conditions. To correct the observations for extinction, zenith transmission coefficients $-\log p = 0.0030$ and 0.0038 were adopted for "good" and "fair" observing conditions, respectively. Within the declination range $-16° \leq \delta \leq 40°$ no change of the aperture efficiency could be detected within the accuracy of our observations.

Most observations were made within ± 2 hours about the meridian. A correction curve relating the true to the indicated position of the 140-foot telescope has been obtained by M. DeJong. We have adopted his curve, checking it for very low and very high declinations with the source positions shown in Table 2.

Several scans in right ascension (α) and declination (δ) were made through the center of each individual source component. Then the sources were mapped using α scans spaced by 3′ in δ. Each α cross-section used to construct the contour maps is an average of at least two observations. The positions of the main components of each source were measured during one single night of excellent observing conditions and within $\pm 15^m$ about the south meridian. When mapping a source, observations were extended in

TABLE 2

ADOPTED SOURCE POSITIONS FOR TELESCOPE POINTING CORRECTIONS

Source	α(1950)	δ(1950)
IC 1795, G133.7+1 2*	$02^h21^m39^s \pm 4^s$	$+51°53'.0 \pm 1'.5$
Sgr A, G0 0−0 0†...	17 42 28 ±4	−28 59 0±1 0
M17, G15 1−0 7‡	18 17 33 ±1	−16 21 1±1 0

* Mezger (1965) unpublished Position measured with the NRAO 300-foot telescope at 1 4 GHz

† Broten, Cooper, Gardner, Minnett, Price, Tonking, and Yabsley (1965) Positions obtained with the Australian 210-foot telescope at 5 GHz

‡ Howard and Maran (1965), α position measured at 9 4 GHz, δ position measured at 2 9 GHz, as quoted by the authors

declination until either no radiation was detectable or until the observed brightness temperature remained constant with declination. This latter slowly varying background radiation was then subtracted from the observed profiles.

The results of our continuum survey are presented in Figure 1 and in Table 3. Columns 1 and 2 give the catalogue numbers of the 22-cm survey (Westerhout 1958) and of the 11-cm survey (Altenhoff, Mezger, Wendker, and Westerhout 1960), respectively. Columns 3, 4, and 5 give optical catalogue numbers of unambiguously identified emission nebulae. Columns 7–10 give the α, δ, and l^{II}, b^{II} coordinates of the sources. Several sources, such as IC 1795, W49 and W51, which were previously considered to be single sources, have been resolved into two and more components. Previously, such subcomponents of a "single" source were designated with A, B, C, etc. However, the example of the Sagittarius region, where the designations A, B, C, etc., are used concurrently with designations A, B1, B2, etc., shows clearly that this type of nomenclature will lead to serious confusion as more results of high-resolution studies of galactic sources become available. We therefore adopted the Australian system, which names a source by its α and δ coordinates (Bolton, Gardner, and Mackey 1964) but used in our case galactic coordinates rather than α and δ coordinates. Galactic coordinates are more appropriate in dealing with predominantly galactic sources and also allow in most cases a considerably shorter designation of a source. To avoid confusion with the Parkes system, the source numbers used here are preceded by a "G." These G-numbers are given in column 6 and will be used throughout the remainder of this paper and Paper II.

Although the unresolved galactic background component has already been removed

© American Astronomical Society • Provided by the NASA Astrophysics Data System

1967ApJ...147..471M

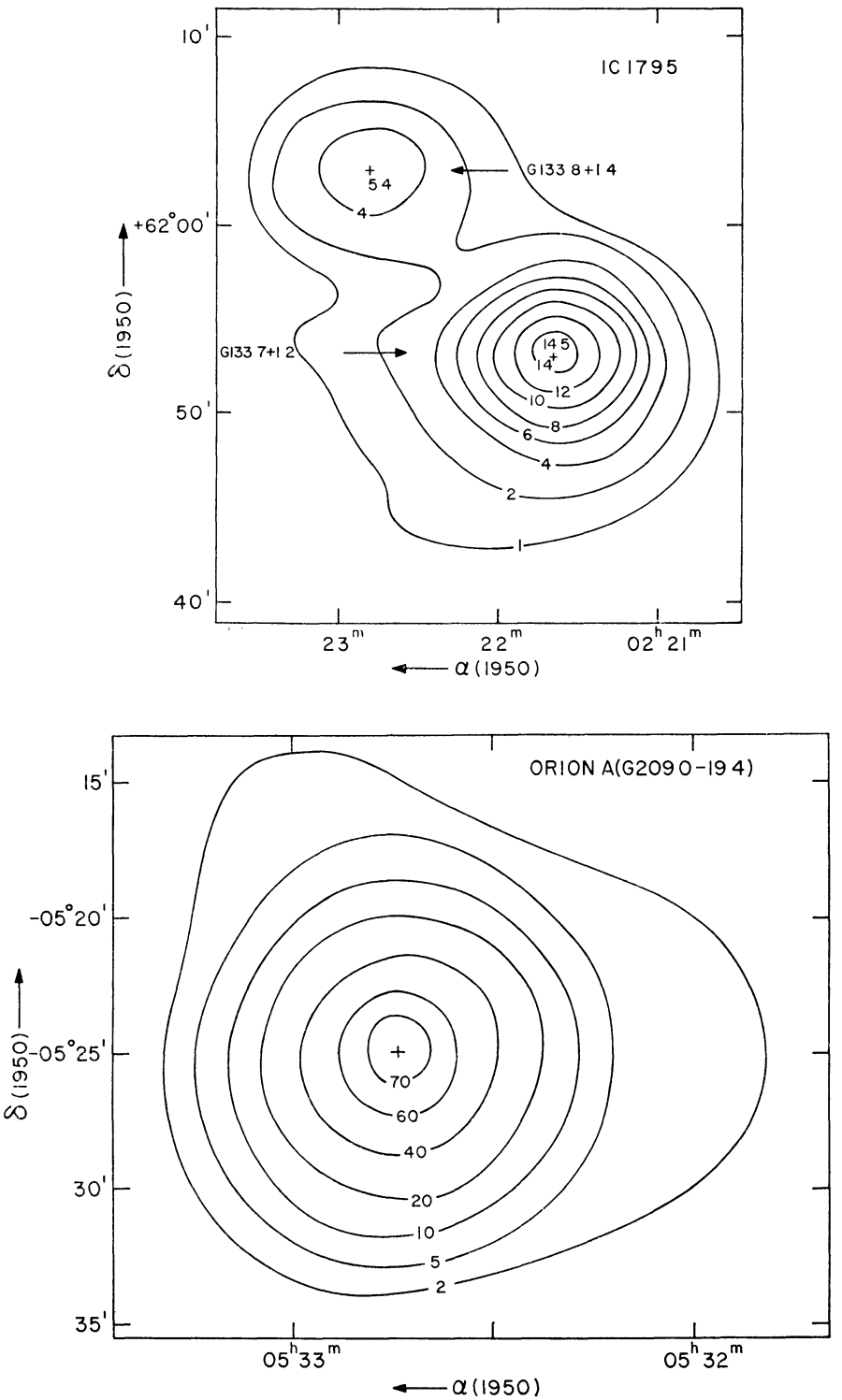

FIG. 1.—Contour maps of galactic radio sources at $\lambda = 6$ cm 1 unit $\widehat{=}$ 1° K $T_A \widehat{=}$ 1.235° K $\overline{T}_b$. Components, which are clearly resolved, are indicated by horizontal arrows and their G-numbers Components, which are not unambiguously resolved, are indicated by oblique arrows.

© American Astronomical Society • Provided by the NASA Astrophysics Data System

1967ApJ...147..471M

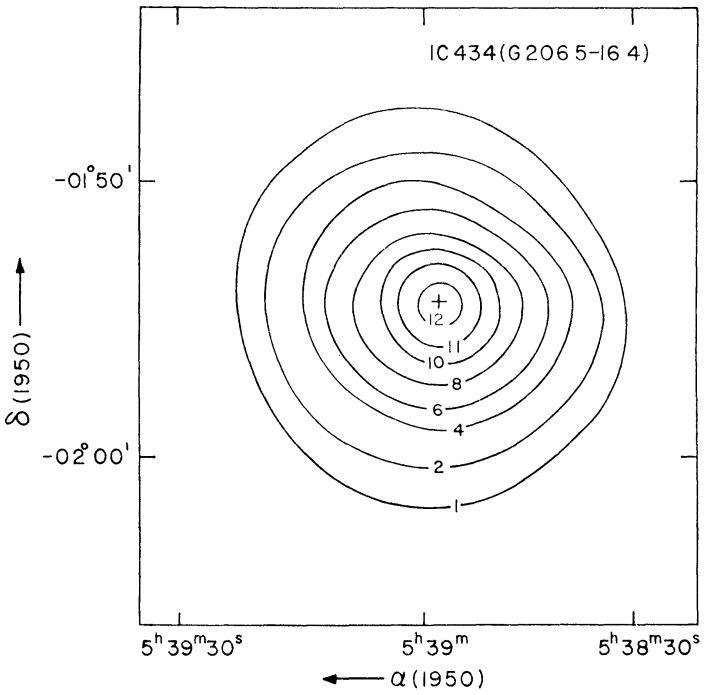

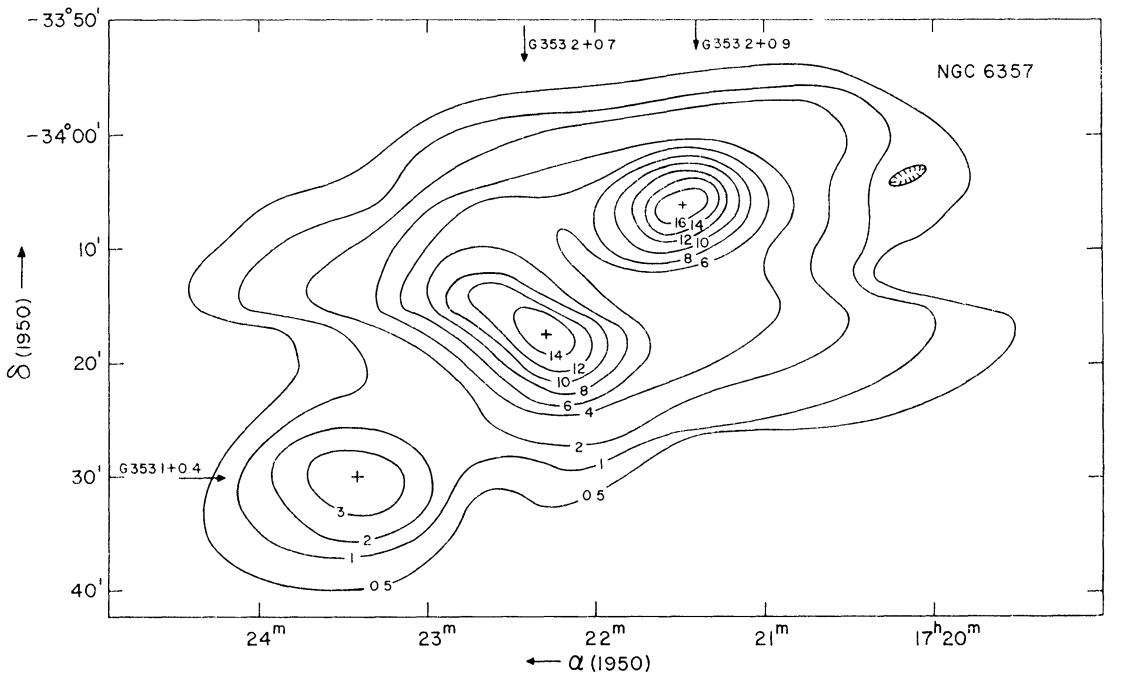

FIG. 1.—*Continued*

© American Astronomical Society • Provided by the NASA Astrophysics Data System

1967ApJ...147..471M

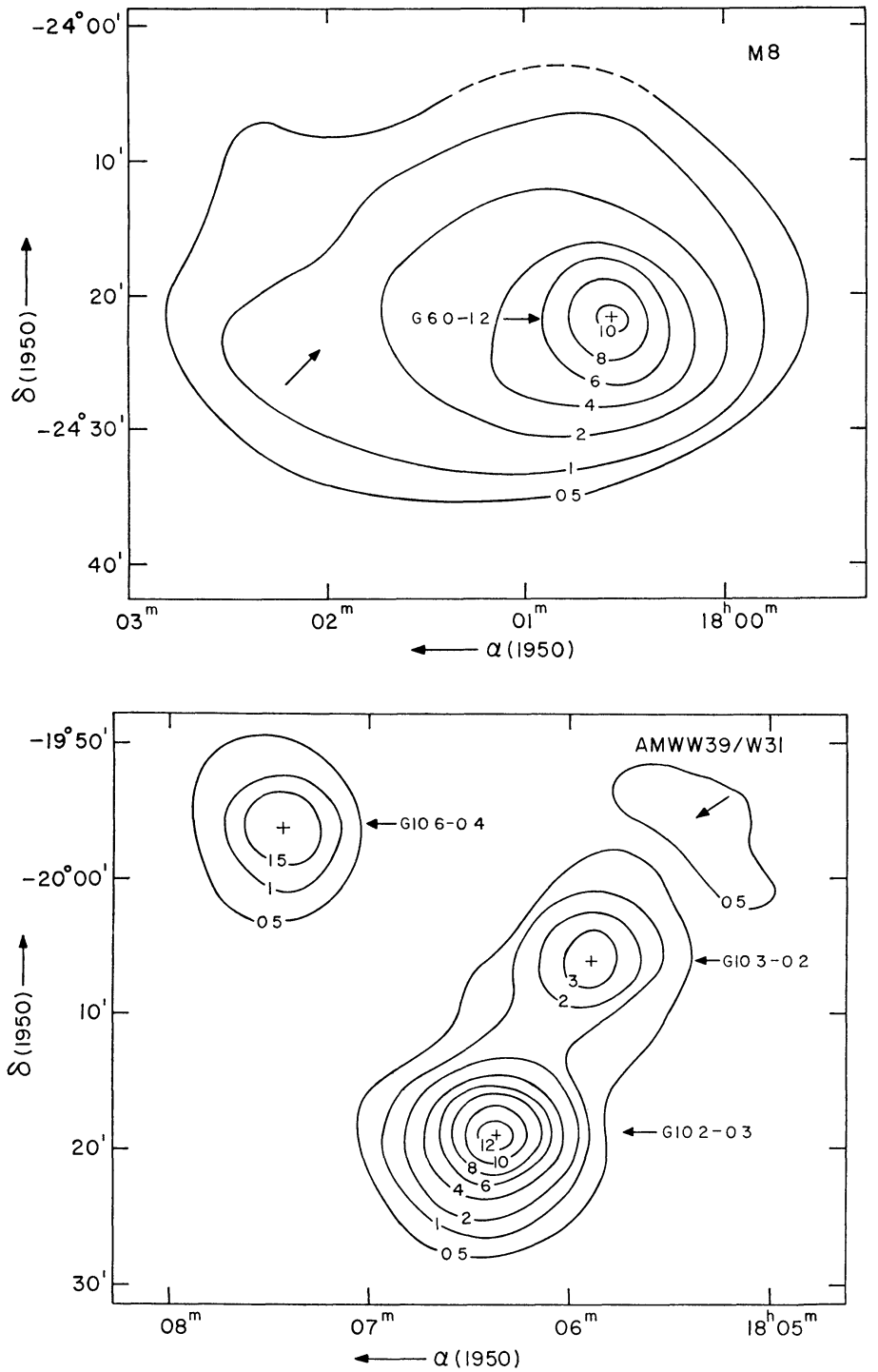

FIG. 1 —*Continued*

© American Astronomical Society • Provided by the NASA Astrophysics Data System

1967ApJ...147..471M

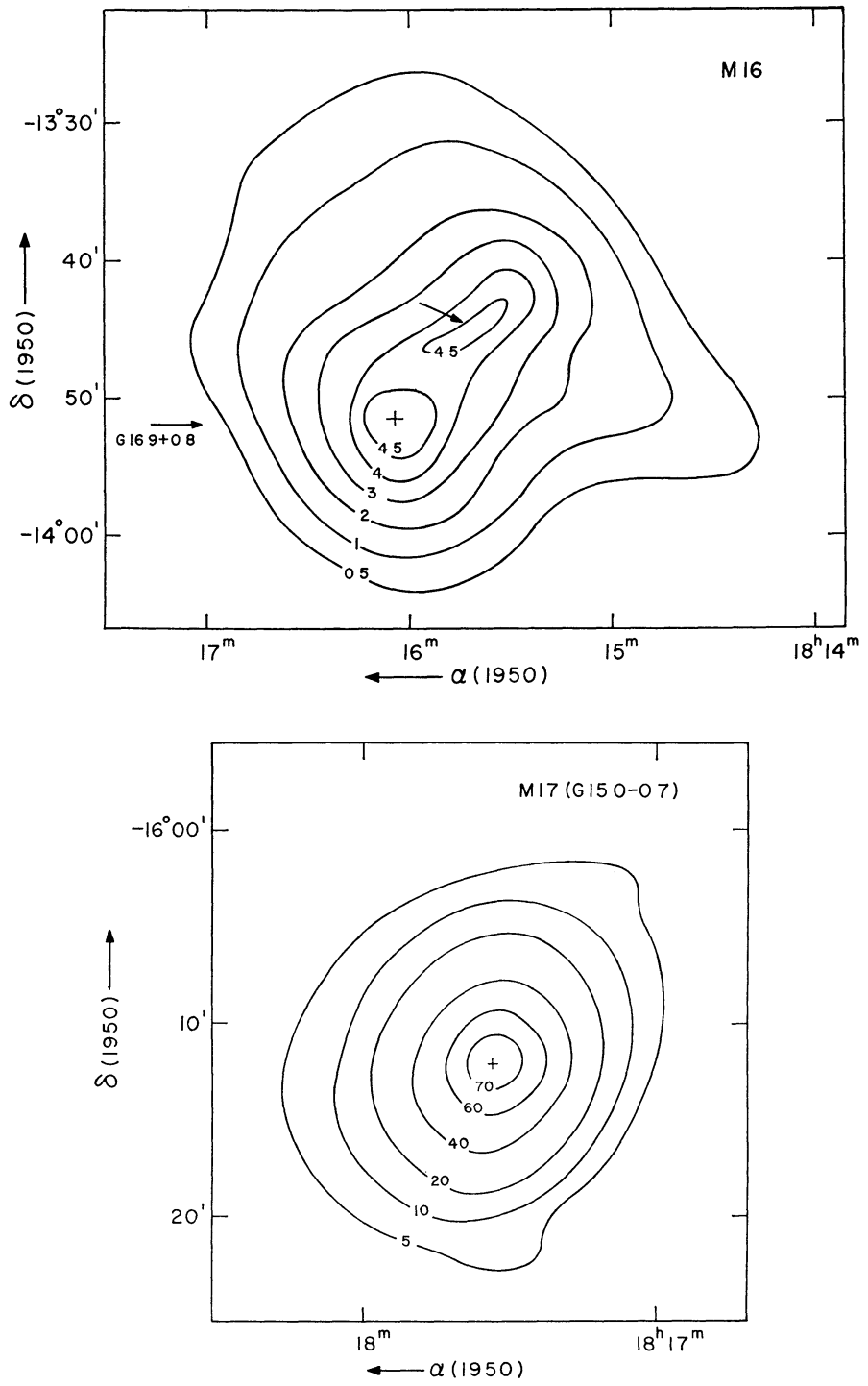

FIG. 1.—*Continued*

© American Astronomical Society • Provided by the NASA Astrophysics Data System

1967ApJ...147..471M

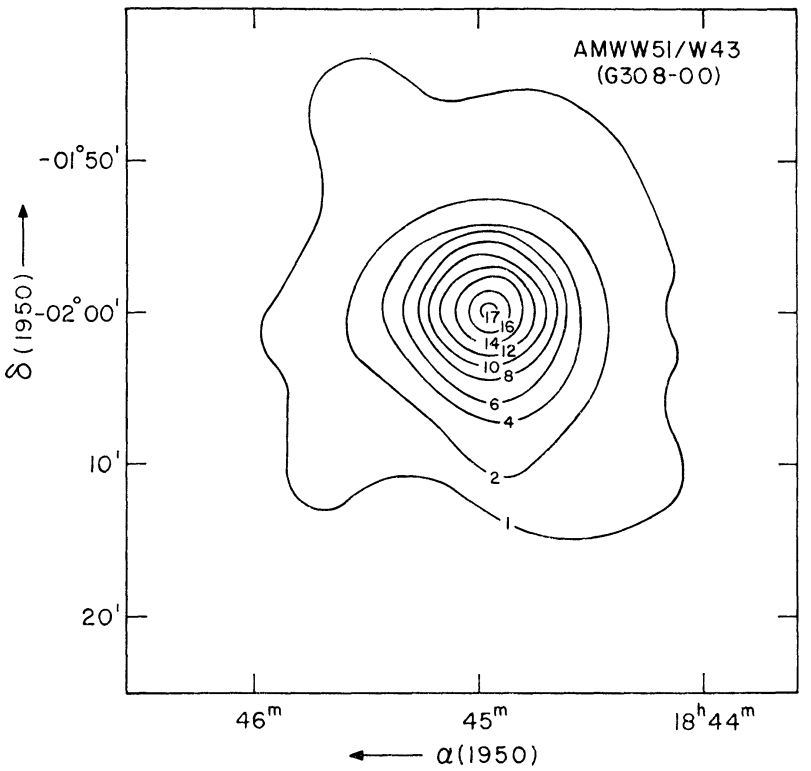

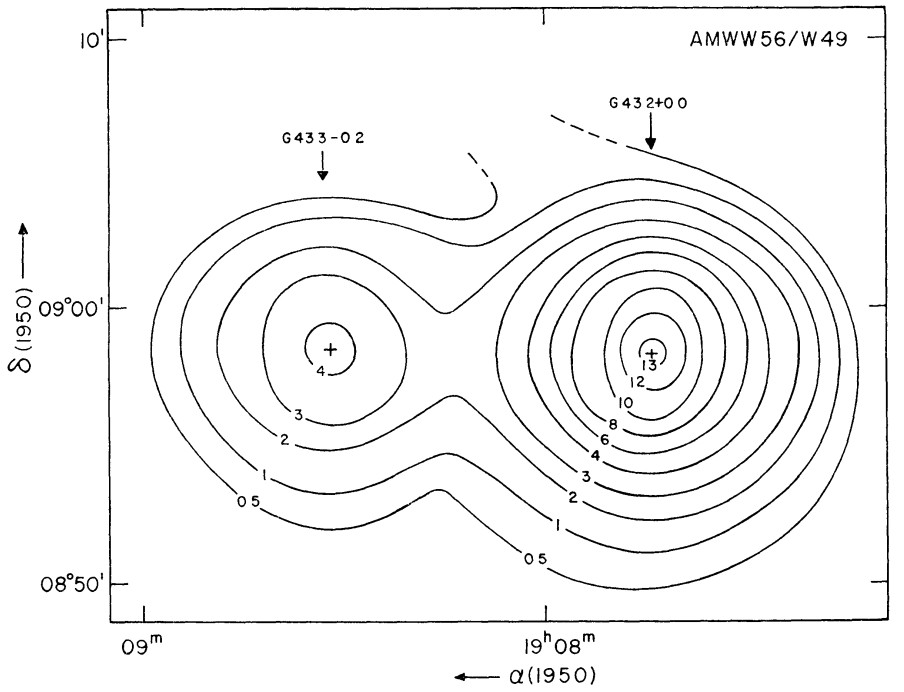

FIG 1—*Continued*

© American Astronomical Society • Provided by the NASA Astrophysics Data System

1967ApJ...147..471M

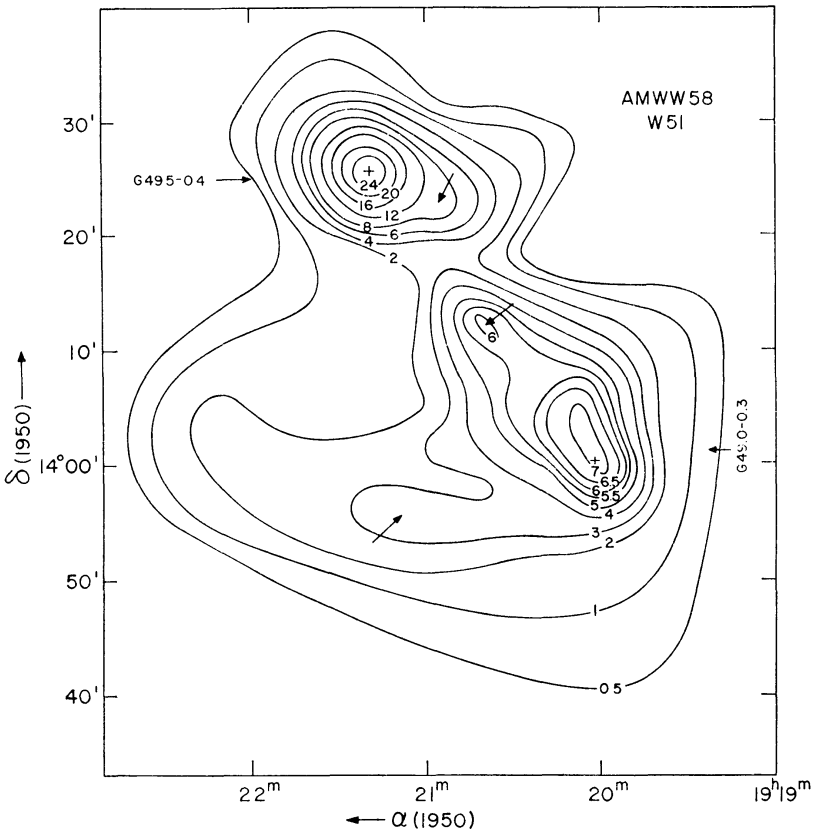

FIG. 1 —*Continued*

from the measured cross-sections, it can be seen from the contour maps that in some cases, e.g., NGC 6357, W31, M8, and W51, one or more strong sources of small angular size are superimposed on a weak but extended background. Since the contribution of the background component to the integrated flux density of the source is nevertheless considerable, we have applied the following reduction method. A Gaussian curve of best fit was computed for the observed α and δ cross-sections through the center of the individual components. With θ_{ob} the HPW of the best-fitting Gaussian curves and θ_A the HPBW of the antenna, the source HPW was computed using the relation valid for the convolution of two Gaussian curves $\theta_s = \sqrt{(\theta_{ob}^2 - \theta_A^2)}$. The source HPW's and the maximum antenna temperatures given in columns 11, 12, and 14 were obtained in this way. We estimate the errors of the quoted apparent source diameters to be between 20 and 50 per cent. In view of this uncertainty, we have used for the following computations the geometrical mean θ_G of the source HPW's, which are given in column 13.

The computation of the flux density values of the individual source components, given in column 15, is then performed by using the relation

$$S_\nu = \frac{8kT_{A_0}}{\eta_A \pi d^2}\left(1 + \frac{\theta_G^2}{\theta_E \theta_H}\right). \tag{3}$$

T_{A_0} is the maximum antenna temperature of the source corrected for atmospheric extinction, as given in column 14. The contour maps were also integrated, and the total flux density of a source was computed using a relation similar to equation (1); this integrated

© American Astronomical Society • Provided by the NASA Astrophysics Data System

1967ApJ...147..471M

TABLE 3

RESULTS OF A CONTINUUM SURVEY OF GALACTIC RADIO SOURCES AT 5007 MHZ

1	2	3	4	5	6	7	8	9	10	11	12	13	14	15	16	17	18	19	
W	AMWW	M	NGC	IC	G	α_{1950}	δ_{1950}	l^{II}	b^{II}	Θ_α	Θ_δ	$\Theta_G = \sqrt{\Theta_\alpha \Theta_\delta}$	T_A(source)	S(source)	$\int B d\Omega$	$S_s/\int B d\Omega$	$\Sigma S_s/\int B d\Omega$	$S_{2.7}$	$S_{14.5}$
										min of arc			°K	10^{-26} W m^{-2} Hz^{-1}		%		10^{-26} W m^{-2} Hz^{-1}	
3	8			1795	133.7 + 1.2	02h 21m 39s ± 4s	+61° 53.0' ± 1.5'	133.68	1.22	3.5	5.3	4.3	14.3	76.5	110 ± 11	70	97		48
					133.8 + 1.4	02h 22m 49s ± 8s	+62° 02.0' ± 3'	133.76	1.40	4.9	4.3	4.6	5.4	30.2		27			
Orion A			1976		209.0 - 19.4	05h 32m 44s ± 4s	-05° 24.9' ± 1'	209.00	-19.40	3.7	4.2	3.9	67.8	342.6	441 ± 30	78		411	342
Orion B			2024	434	206.5 - 16.4	05h 38m 58s ± 8s	-01° 54.2' ± 2'	206.48	-16.39	4.2	3.9	4.0	11.8	60.5	63 ± 7	96		51	
22	30		6357		353.2 + 0.9	17h 21m 29s ± 8s	-34° 06.2' ± 2'	353.22	0.91	8.0	8.3	8.2	16.0	156.2	477 ± 50	33	88	300	
					353.2 + 0.7	17h 22m 21s ± 8s	-34° 17.6' ± 2'	353.16	0.66	12.1	9.9	10.9	14.9	215.0		45			
					353.1 + 0.4	17h 23m 21s ± 12s	-34° 30.0' ± 3'	353.11	0.37	9.3	9.9	9.6	3.9	46.9		10			
Sgr A					0.0 - 0.0	17h 42m 28s ± 4s	-28° 59.0' ± 1'	359.95	-0.04				37.0					341	136
					0.2 - 0.1	17h 43m 08s ± 12s	-28° 47.8' ± 3'	0.18	-0.07				10.8						233
					0.6 - 0.1	17h 44m 06s ± 12s	-28° 26.6' ± 3'	0.59	-0.06				8.4						
					0.7 - 0.1	17h 44m 17s ± 12s	-28° 22.2' ± 3'	0.68	-0.06				11.8						
29	37	8	6523		6.0 - 1.2	18h 00m 34s ± 8s	-24°21.9' ± 2'	5.98	-1.16	8.7	8.3	8.5	9.7	99.1	189 ± 30	52		117	
31	39				10.3 - 0.2	18h 05m 57s ± 12s	-20° 08.4' ± 3'	10.27	-0.16	5.0	---	5.0*	3.4	20.2	101 ± 20	20	92	58	
					10.2 - 0.3	18h 06m 22s ± 8s	-20° 19.2' ± 2'	10.16	-0.33	3.8	4.0	3.9	12.5	63.2		63			
					10.6 - 0.4	18h 07m 28s ± 12s	-19° 56.3' ± 3'	10.62	-0.37	3.9	---	3.9*	1.7	8.6		9			
37	42	16	6611		16.9 + 0.8	18h 16m 04s ± 12s	-13° 51.6' ± 2'	16.93	0.75	4.9	15.4*	8.7	5.0	52.6	154 ± 25	34		65	
Omega Nebula		17	6618		15.0 - 0.7	18h 17m 33s ± 4s	-16° 12.1' ± 1'	15.05	-0.67	5.1	6.8	5.9	73.3	500.4	621 ± 60	81		554	527
43	51				30.8 - 0.0	18h 44m 57s ± 8s	-01° 59.6' ± 2'	30.76	-0.02	4.9	5.5	5.2	16.0	98.0	198 ± 20	50		125	86
49	56				43.2 + 0.0	19h 07m 44s ± 4s	09° 01.7' ± 1'	43.16	0.04	3.4	2.8	3.1	12.7	57.7	80 ± 10	72	100	58	
					43.3 - 0.2	19h 08m 38s ± 8s	09° 01.9' ± 2'	43.27	-0.16	4.2	4.0	4.1	4.2	22.1		28			
51	58				49.0 - 0.3	19h 20m 04s ± 12s	14° 02.2' ± 3'	49.00	-0.27				6.5		402 ± 50				
					49.5 - 0.4	19h 21m 19s ± 4s	14° 25.7' ± 2'	49.49	-0.35	4.9	3.8	4.3	21.8	116.6		29		153	108
75	71	Cygnus Reg.			81.7 + 0.5	20h 37m 30s ± 12s	42° 10.0' ± 3'	81.72	0.51				5.9					65	

* Adopted values; no gaussian fit possible.

© American Astronomical Society • Provided by the NASA Astrophysics Data System

1967ApJ...147..471M

flux density is given in column 16. The ratios of the flux density of the individual source components and of the sum of the source components constituting a source to the integrated flux density are given in columns 17 and 18. In column 19 the flux density values obtained at 11 cm (Altenhoff *et al.* 1960) and at 2 cm (Baars *et al.* 1965*a*) are given. It is obvious that in these earlier surveys in many cases only the bright central core of an extended source or the strongest component of an association of two or more sources had been measured.

The Sagittarius and the Cygnus X regions have not been mapped in this survey, since this had already been done by others (Broten *et al.* 1965; Wendker 1966). Only those parameters needed for the reduction of our recombination-line observations are therefore given for these sources.

IV. TOTAL MASS AND DENSITY OF THE IONIZED HYDROGEN IN H II REGIONS

The intensity of the radiation emitted from a point x,y (cartesian angular coordinates) on the surface of the H II region is described by the equivalent brightness temperature $T_b(x,y)$ of this point. This is related to the optical depth τ_C of the free-free radiation and the electron temperature T_e by the relation

$$T_b(x,y) = T_e(x,y)\,\{1 - \exp\,[-\tau_C(x,y)]\} \approx T_e(x,y)\tau_C(x,y) \text{ for } \tau_C \ll 1\,. \tag{4}$$

The condition $\tau_C \ll 1$ at the frequency 5 GHz is a valid assumption. The optical path length for free-free emission at the frequency $\nu = 5009$ MHz is given by the exact equation (A.1a) (Appendix) and its approximation equation (A.1b) which we will use throughout both this paper and Paper II. In order to simplify the problem we assume for the further computations a constant average value for the electron temperature. The x,y dependence of the brightness temperature is therefore contained only in the density distribution of the ionized hydrogen $N(x,y,r)$:

$$T_b = 8.235 \times 10^{-2} a \left(\frac{T_e}{^\circ\mathrm{K}}\right)^{-0.35} \left(\frac{\nu}{\mathrm{GHz}}\right)^{-2.1} \int N^2(x,y,r)\,dr\,. \tag{5}$$

The correction factor a in this equation is defined by (A.2) in the Appendix and listed in Table 6 (see below) as a function of both frequency and electron temperature. Substituting this factor permits the evaluation of equation (5) and following equations with the exact formula for the optical path length for free-free emission. The factor a is kept in the general equations for electron density, total mass of ionized hydrogen, and emission measure derived in the Appendix. However, we shall set $a = 1$ when applying these equations to our observations.

Since the brightness temperature of an H II region depends on the square of the electron density, any determination of the total mass and the average density of the ionized hydrogen will depend very strongly on the density-distribution model used for the evaluation of the observations. Following common procedures, we adopt the following models to describe H II regions:

MODEL I	Constant density N_0 within the sphere of apparent diameter θ_{sph}. Zero density elsewhere.
MODEL II	Constant density N_0 within a cylinder of apparent diameter θ_{cyl}, whose axis of symmetry is parallel to the r-axis and whose length is equal to its diameter. Zero density elsewhere.
MODEL III	An exponentially tapered distribution, whose maximum density is N_0. The apparent half-power width of the square of this distribution is θ_G.

Such symmetrical density models may be appropriate for the central region of Orion A or IC 434, but certainly are not valid in general, e.g., NGC 6357 and W51 (see Fig. 1).

© American Astronomical Society • Provided by the NASA Astrophysics Data System

1967ApJ...147..471M

Not to depart too much from reality, we restrict our computation of mass and density to the bright parts of the investigated emission nebulae. The mass of ionized hydrogen derived in this way will be, in most cases, considerably smaller than the total mass of ionized hydrogen of the investigated H II region. However, combining the results of Papers I and II, we will get at least a set of consistent physical parameters (mass, density, electron temperature, and internal turbulence) for these selected areas.

When we replace the linear dimension by apparent angles through the relations

$$\theta = (x^2 + y^2)^{1/2}/D\,; \qquad \phi = r/D\,,$$

with D the distance of the H II region, equation (5) assumes the form

$$T_b = 82.35\,a \left(\frac{\nu}{\mathrm{GHz}}\right)^{-2\,1} \left(\frac{D}{\mathrm{kpc}}\right) \left(\frac{T_e}{^\circ\mathrm{K}}\right)^{-0\,35} \int N^2(\theta,\phi)\,d\phi\,. \tag{6}$$

TABLE 4

MODEL CONVERSION FACTORS FOR COMPUTING TOTAL MASS ELECTRON DENSITY, AND EMISSION MEASURE

	u_1 (Density)	u_2 (Mass)	u_3 (Emission Measure)
Model I (sphere)	0 775	1 291	1 471
Model II (cylinder)	857	1 167	1 201
Model III (gauss) .	0 911	3 106	1 065

Equation (6) is evaluated in the Appendix for the above density models. Substituting $a = 1$ and $\nu = 5.009$ GHz in equation (A.13) yields the relation

$$\left(\frac{N_0}{\mathrm{cm}^{-3}}\right) = u_1 6.884 \times 10^2 \left(\frac{T_e}{10^4\,^\circ\mathrm{K}}\right)^{0\,175} \left(\frac{S_{5\ \mathrm{GHz}}}{\mathrm{f.u.}}\right)^{0\,5} \left(\frac{D}{\mathrm{kpc}}\right)^{-0\,5} \left(\frac{\theta_G}{\mathrm{min\ arc}}\right)^{-1\,5}, \tag{7}$$

which allows us to compute the average electron density of an H II region if its flux density $S_{5\ \mathrm{GHz}}$, its apparent Gaussian HPW θ_G, its electron temperature T_e, and its distance D are known. Integration of the density distribution and multiplication of the result with the ratio of the mass m_H of a hydrogen atom to the solar mass $M_\odot$ yields the total mass of ionized hydrogen, expressed in solar masses (eq. [A.14], Appendix). Substituting again $a = 1$ and $\nu = 5.009$ GHz yields

$$M/M_\odot = u_2\ 0.419 \left(\frac{T_e}{10^4\,^\circ\mathrm{K}}\right)^{0.175} \left(\frac{S_{5\ \mathrm{GHz}}}{\mathrm{f.u.}}\right)^{0\,5} \left(\frac{D}{\mathrm{kpc}}\right)^{2\,5} \left(\frac{\theta_G}{\mathrm{min\ arc}}\right)^{1\,5}. \tag{8}$$

The maximum emission measure in the center of the source is

$$E_{\max} = \int N^2 dr = D \int N^2 d\phi = u_3\ 0.291 \left(\frac{D}{\mathrm{kpc}}\right) \left(\frac{\theta_G}{\mathrm{min\ arc}}\right) \left(\frac{N_0}{\mathrm{cm}^{-3}}\right)^2. \tag{9}$$

In these calculations 1 flux unit (f.u.) equals 10^{-26} W m^{-2} Hz^{-1}.

The numerical values of the factors u_1, u_2, and u_3 depend on the particular model chosen for the density distribution of the H II region. They are compiled in Table 4.

The values for mass and density of the ionized hydrogen derived from equations (7) and (8) differ only slightly from the spherical and cylindrical models. The average densities of these two models are also in good agreement with the maximum electron density in the center of the Gaussian density distribution. But since in this latter model the density

© American Astronomical Society • Provided by the NASA Astrophysics Data System

1967ApJ...147..471M

decreases with the distance from the center, it is clear that a larger total mass of ionized hydrogen is required in order to produce the same flux density as the models with constant density. Moreover, it is clear from the way equations (7) and (8) have been derived that the maximum emission measure is independent of the particular model. Equations (7), (8), and (9) were evaluated for:

i) A spherical density model (Model I).
ii) An electron temperature of $\langle T_e \rangle = 5820°$ K, which is a mean value of the electron temperatures given in Paper II, Table 2, column 7, if the off-center values observed for Orion A and M 17 and the electron temperature of W51, G 49.0 − 0.3 are omitted.
iii) The apparent source diameters θ_G, given in Table 3, column 13, of this paper.
iv) The distances D given in Table 2, column 5, of Paper II.
v) The flux densities given in Table 3, column 15, of this paper.

The results of these computations are given in Table 5. The linear diameters $2R$ of the spherical H II regions (col. 5, Table 5) have been computed using the relation $\theta_{\text{sph}} D = 1.471\ \theta_G D$ (eq. [A.10], Appendix). The distance z of the H II regions from the galactic plane (col. 6, Table 5) has been computed using the relation $z = (\sin b^{\text{II}}) D$.

V. CONCLUSIONS

Before discussing the figures given in Table 5 in more detail, we want to reiterate that we have restricted our computations to the brightest and hence the most dense parts of the investigated H II regions. When compared with earlier optical and radio measurements, the total masses of ionized hydrogen listed in column 9 of Table 5 and the diameters listed in column 5 may thus be considerably lower. Likewise, the electron densities given in column 8 may be considerably higher. The largest uncertainty in the computation of M and N_0 arises from our assumption of a smooth density distribution in the H II region (which is certainly only a very crude approximation of the true density distribution) and not from observational errors. We therefore do not quote errors for these quantities. For the emission measures communicated in column 10 of Table 5 we estimate a maximum error of ± 5 per cent.

In summary, the evaluation of our observations yields the following results:

i) The diameters of the H II regions (Table 5, col. 5) vary from 0.69 pc (IC 434) to 18.7 pc (W49, G43.2 + 0.0). The mean value of all z-distances (col. 6) is −13.7 pc; the rms deviation of the z-distances of 16 H II regions from the galactic plane is 57.8 pc.
ii) Electron densities (col. 8) were found to extend from 1649 cm^{-3} (Orion A) to 87 cm^{-3} (M16).
iii) The total masses of ionized hydrogen (col. 9) range from 3 $M_\odot$ (IC 434) to 15230 $M_\odot$ (W49, G 43.2 + 0.0).
iv) The emission measures in the center of those sources whose recombination-line radiation has been observed (col. 10) lie in the range 2.3×10^6 (Orion A) to 7.0×10^4 (M16).

These are average values for the brightest parts in the radio brightness distribution of the investigated H II regions. For the computation of these average values we have assumed a constant or exponentially decreasing electron density distribution within the solid source angle. This assumption is in most cases only a very crude approximation. In a recent survey at a wavelength $\lambda = 2$ cm with the NRAO 140-foot telescope (angular resolution 2′) we have found that most of these bright peaks are resolved into two or more components. If this result is taken into account, the electron densities and emission measures should increase, whereas the total mass of ionized hydrogen should decrease.

It is an intriguing question as to what angular resolution would ultimately resolve all

© American Astronomical Society • Provided by the NASA Astrophysics Data System

1967ApJ...147..471M

TABLE 5

PHYSICAL PARAMETERS OF THE BRIGHT CENTERS OF SOME GALACTIC HII-REGIONS

1	2	3	4	5	6	7	8	9	10
Source	Component	θ_G	D	2R	Z	$S_{5\ GHz}$	N_e	$M/M_\odot$	E_{max}
		min arc	kpc	pc	pc	10^{-26} Wm^{-2} Hz^{-1}	cm^{-3}		pc x cm^{-6}
IC 1795	G133.7+1.2	4.3	2.6	4.78	55.2	76.5	295	418	$4.2 \cdot 10^5$
	G133.8+1.4	4.6	2.6	5.12	63.7	30.2	168	291	$1.4 \cdot 10^5$
Orion A	G209.0-19.4	3.9	0.5	0.83	-166.1	342.6	1649	12	$2.3 \cdot 10^6$
IC 434	G206.5-16.4	4.0	0.4	0.69	-112.9	60.5	746	3	$3.8 \cdot 10^5$
NGC 6357	G353.2+0.9	8.2	1.0	3.51	15.9	156.2	258	144	$2.3 \cdot 10^5$
	G353.2+0.7	10.9	1.0	4.66	11.5	215.0	198	260	$1.8 \cdot 10^5$
	G353.1+0.4	9.6	1.0	4.11	6.5	46.9	112	100	$5.1 \cdot 10^4$
M 8	G 6.0-1.2	8.5	1.1	4.00	-22.2	99.1	186	154	$1.4 \cdot 10^5$
W 31	G 10.3-0.2	5.0	2.1	4.49	-5.9	20.2	135	158	$8.1 \cdot 10^4$
	G 10.2-0.3	3.9	2.1	3.50	-12.2	63.2	346	192	$4.2 \cdot 10^5$
	G 10.6-0.4	3.9	2.1	3.50	-13.7	8.6	127	71	$5.7 \cdot 10^4$
M 16	G 16.9+0.8	8.7	2.5	9.31	32.9	52.6	87	905	$7.0 \cdot 10^4$
M 17	G 15.0-0.7	5.9	1.8	4.54	-21.2	500.4	565	685	$1.5 \cdot 10^6$
W 43	G 30.8-0.0	5.2	6.5	14.46	-2.3	98.0	159	6220	$3.7 \cdot 10^5$
W 49	G 43.2+0.0	3.1	14.1	18.70	8.7	57.7	180	15230	$6.1 \cdot 10^5$
W 51	G 49.0-0.3	---	6.5	---	-31.1	---	---	---	---
	G 49.5-0.4	4.3	6.5	11.96	-40.2	116.6	231	5100	$6.4 \cdot 10^5$

© American Astronomical Society • Provided by the NASA Astrophysics Data System

1967ApJ...147..471M

subcomponents of the distant and giant H II regions component G43.2 + 0.0 of W49 and component G49.5 − 0.4 of W51. Observations with the NRAO interferometer at $\lambda = 11$ cm show that an angular resolution of 20″ is still not adequate for complete resolution; both of the above source components still show very complex structure.

It is a pleasure to thank J. Schraml for his assistance in the reduction of our observations and to thank the operators and mechanics of the NRAO 140-foot telescope for their excellent co-operation in performing these observations. We thank W. Tyler for providing the preliminary interferometer observations of W49 and W51.

APPENDIX

The optical path length for free-free emission is given by

$$\tau_c(\text{Oster}) = 3.014 \times 10^{-2} \left(\frac{T_e}{^\circ\text{K}}\right)^{-1.5} \left(\frac{\nu}{\text{GHz}}\right)^{-2.0} \left\{\ln\left[4.955 \times 10^{-2} \left(\frac{\nu}{\text{GHz}}\right)^{-1}\right] + 1.5 \ln\left(\frac{T_e}{^\circ\text{K}}\right)\right\} \left(\frac{E}{\text{pc} \cdot \text{cm}^{-6}}\right). \quad \text{(A.1a)}$$

This equation was derived by Oster (1961). The approximation

$$\tau_c(\text{AMWW}) = 8.235 \times 10^{-2} \left(\frac{T_e}{^\circ\text{K}}\right)^{-1.35} \left(\frac{\nu}{\text{GHz}}\right)^{-2.1} \left(\frac{E}{\text{pc} \cdot \text{cm}^{-6}}\right) \quad \text{(A.1b)}$$

is given by Altenhoff *et al.* (1960). In both equations $N_i = N_e$ and $Z = 1$; the emission measure $E = \int N_e^2 ds$ has dimensions pc cm^{-6}. We define a factor a as the ratio of equation (A.1a) to equation (A.1b);

$$a = \frac{\tau_c(\text{Oster})}{\tau_c(\text{AMWW})} = 0.366 \left(\frac{\nu}{\text{GHz}}\right)^{0.1} \left(\frac{T_e}{^\circ\text{K}}\right)^{-0.15} \left\{\ln\left[4.995 \times 10^{-2} \left(\frac{\nu}{\text{GHz}}\right)^{-1}\right] + 1.5 \ln\left(\frac{T_e}{^\circ\text{K}}\right)\right\}. \quad \text{(A.2)}$$

This factor measures the deviation between the exact formula and its approximation. Table 6 lists the factor a for the temperature range $3 \times 10^3 \leq T_e \leq 1.5 \times 10^4$ ° K and the frequency range 100 MHz $\leq \nu \leq$ 100 GHz.

In no case does the approximation deviate more than 24 per cent from the exact expression. In the region of principal interest $5 \times 10^3 \leq T_e \leq 1.2 \times 10^4$ ° K and 100 MHz $\leq \nu \leq$ 35 GHz the deviation is less than 10 per cent. Considering the observational errors which enter into the computation of the physical parameters of an H II region, we can in most cases set $a \approx 1$ and consequently τ_c (AMWW) = τ_c (Oster). However, to permit more accurate computations we have kept the factor a in the general equations derived below. We shall set $a = 1$ when applying these equations to our observations.

Evaluating the integral in equation (6) for the following density distributions

$$\begin{aligned} N(\theta,\phi) &= N_0 \text{ for } \sqrt{(\theta^2 + \phi^2)} \leq \frac{\theta_{\text{sph}}}{2} && \text{Model I} \\ &= 0 \text{ elsewhere} \\ &= N_0 \text{ for } \theta \leq \frac{\theta_{\text{cyl}}}{2} \text{ and } 0 \leq \phi \leq \theta_{\text{cyl}} && \text{Model II} \\ &= 0 \text{ elsewhere} \\ &= N_0 \exp\left[-(\theta^2 + \phi^2)/2(0.6\,\theta_G)^2\right] && \text{Model III ;} \end{aligned} \quad \text{(A.3)}$$

© American Astronomical Society • Provided by the NASA Astrophysics Data System

1967ApJ...147..471M

TABLE 6

The Ratio $\underline{a} = \tau_c$ (Oster)/τ_c (AMWW) as a Function of Frequency and Electron Temperature

FREQUENCY (MHZ)	ELECTRON TEMPERATURE (DEGREE K) 3,000	4,000	5,000	6,000	7,000	8,000	9,000	10,000	11,000	12,000	13,000	14,000	15,000
100	0.9893	0.9837	0.9784	0.9736	0.9691	0.9651	0.9613	0.9577	0.9544	0.9513	0.9484	0.9456	0.9430
200	0.9953	0.9920	0.9884	0.9849	0.9815	0.9782	0.9751	0.9722	0.9694	0.9668	0.9643	0.9619	0.9596
300	0.9969	0.9951	0.9927	0.9900	0.9872	0.9845	0.9819	0.9794	0.9770	0.9747	0.9724	0.9703	0.9683
400	0.9971	0.9965	0.9949	0.9928	0.9906	0.9883	0.9860	0.9838	0.9817	0.9796	0.9776	0.9757	0.9738
500	0.9966	0.9970	0.9961	0.9945	0.9927	0.9908	0.9888	0.9869	0.9850	0.9831	0.9813	0.9795	0.9778
600	0.9959	0.9971	0.9967	0.9956	0.9942	0.9926	0.9909	0.9891	0.9874	0.9857	0.9840	0.9824	0.9808
700	0.9950	0.9969	0.9970	0.9963	0.9952	0.9938	0.9924	0.9908	0.9893	0.9877	0.9862	0.9846	0.9831
800	0.9940	0.9965	0.9971	0.9968	0.9959	0.9948	0.9935	0.9921	0.9907	0.9893	0.9879	0.9864	0.9850
900	0.9929	0.9960	0.9970	0.9970	0.9964	0.9955	0.9944	0.9932	0.9919	0.9906	0.9893	0.9879	0.9866
1,000	0.9918	0.9955	0.9968	0.9971	0.9967	0.9960	0.9951	0.9940	0.9929	0.9917	0.9904	0.9892	0.9880
2,000	0.9812	0.9885	0.9926	0.9949	0.9962	0.9969	0.9971	0.9970	0.9968	0.9964	0.9958	0.9953	0.9946
3,000	0.9719	0.9817	0.9875	0.9912	0.9935	0.9951	0.9961	0.9967	0.9970	0.9971	0.9971	0.9969	0.9966
4,000	0.9639	0.9755	0.9826	0.9873	0.9905	0.9927	0.9943	0.9954	0.9961	0.9966	0.9969	0.9971	0.9971
5,000	0.9568	0.9699	0.9780	0.9835	0.9874	0.9902	0.9922	0.9938	0.9949	0.9957	0.9963	0.9967	0.9969
6,000	0.9504	0.9647	0.9738	0.9800	0.9844	0.9877	0.9901	0.9920	0.9934	0.9945	0.9953	0.9959	0.9964
7,000	0.9445	0.9599	0.9698	0.9766	0.9815	0.9852	0.9880	0.9902	0.9919	0.9932	0.9942	0.9950	0.9957
8,000	0.9391	0.9555	0.9661	0.9734	0.9788	0.9828	0.9859	0.9884	0.9903	0.9918	0.9931	0.9940	0.9948
9,000	0.9341	0.9513	0.9625	0.9704	0.9762	0.9805	0.9839	0.9866	0.9887	0.9905	0.9919	0.9930	0.9939
10,000	0.9293	0.9474	0.9592	0.9675	0.9736	0.9783	0.9819	0.9848	0.9872	0.9891	0.9906	0.9919	0.9930
11,000	0.9249	0.9437	0.9560	0.9648	0.9712	0.9762	0.9800	0.9831	0.9856	0.9877	0.9894	0.9908	0.9920
12,000	0.9207	0.9402	0.9530	0.9621	0.9689	0.9741	0.9782	0.9815	0.9842	0.9864	0.9882	0.9897	0.9910
13,000	0.9167	0.9368	0.9501	0.9596	0.9666	0.9721	0.9764	0.9798	0.9827	0.9850	0.9870	0.9886	0.9900
14,000	0.9129	0.9336	0.9473	0.9571	0.9645	0.9701	0.9746	0.9783	0.9812	0.9837	0.9858	0.9876	0.9891
15,000	0.9093	0.9305	0.9447	0.9548	0.9624	0.9682	0.9729	0.9767	0.9798	0.9824	0.9846	0.9865	0.9881
16,000	0.9058	0.9276	0.9421	0.9525	0.9603	0.9664	0.9713	0.9752	0.9785	0.9812	0.9835	0.9854	0.9871
17,000	0.9024	0.9247	0.9396	0.9503	0.9584	0.9646	0.9697	0.9737	0.9771	0.9800	0.9823	0.9844	0.9861
18,000	0.8992	0.9220	0.9372	0.9482	0.9565	0.9629	0.9681	0.9723	0.9758	0.9787	0.9812	0.9834	0.9852
19,000	0.8961	0.9193	0.9349	0.9461	0.9546	0.9612	0.9666	0.9709	0.9745	0.9776	0.9801	0.9823	0.9843
20,000	0.8930	0.9167	0.9326	0.9441	0.9528	0.9596	0.9651	0.9695	0.9733	0.9764	0.9791	0.9813	0.9833
25,000	0.8793	0.9049	0.9223	0.9349	0.9444	0.9520	0.9581	0.9631	0.9673	0.9709	0.9739	0.9766	0.9789
30,000	0.8672	0.8946	0.9131	0.9266	0.9370	0.9451	0.9518	0.9573	0.9619	0.9658	0.9692	0.9721	0.9747
35,000	0.8565	0.8853	0.9049	0.9192	0.9302	0.9389	0.9460	0.9519	0.9569	0.9611	0.9648	0.9680	0.9708
40,000	0.8467	0.8768	0.8973	0.9124	0.9239	0.9332	0.9407	0.9470	0.9523	0.9568	0.9607	0.9642	0.9672
45,000	0.8378	0.8690	0.8904	0.9061	0.9182	0.9278	0.9357	0.9423	0.9479	0.9527	0.9569	0.9605	0.9637
50,000	0.8295	0.8618	0.8839	0.9002	0.9128	0.9229	0.9311	0.9380	0.9438	0.9489	0.9532	0.9571	0.9604
55,000	0.8218	0.8550	0.8778	0.8947	0.9077	0.9182	0.9267	0.9339	0.9400	0.9452	0.9498	0.9538	0.9573
60,000	0.8145	0.8487	0.8722	0.8895	0.9030	0.9137	0.9226	0.9300	0.9363	0.9418	0.9465	0.9507	0.9544
65,000	0.8077	0.8427	0.8668	0.8846	0.8984	0.9095	0.9186	0.9263	0.9328	0.9385	0.9434	0.9477	0.9515
70,000	0.8012	0.8370	0.8616	0.8799	0.8941	0.9055	0.9149	0.9228	0.9295	0.9353	0.9404	0.9448	0.9488
75,000	0.7950	0.8316	0.8568	0.8755	0.8900	0.9017	0.9113	0.9194	0.9263	0.9323	0.9375	0.9421	0.9462
80,000	0.7892	0.8264	0.8521	0.8712	0.8861	0.8980	0.9079	0.9161	0.9232	0.9293	0.9347	0.9394	0.9436
85,000	0.7836	0.8214	0.8477	0.8671	0.8823	0.8945	0.9045	0.9130	0.9203	0.9265	0.9320	0.9369	0.9412
90,000	0.7782	0.8167	0.8434	0.8632	0.8786	0.8911	0.9014	0.9100	0.9174	0.9238	0.9295	0.9344	0.9388
95,000	0.7730	0.8121	0.8392	0.8594	0.8751	0.8878	0.8983	0.9071	0.9147	0.9212	0.9270	0.9320	0.9366
100,000	0.7680	0.8077	0.8353	0.8558	0.8717	0.8846	0.8953	0.9043	0.9120	0.9187	0.9245	0.9297	0.9343

© American Astronomical Society • Provided by the NASA Astrophysics Data System

1967ApJ...147..471M

we obtain

$$\begin{aligned}\int N^2(\theta,\phi)d\phi &= N_0{}^2\theta_{\rm sph}(1-4\theta^2/\theta^2_{\rm sph}) = N_0{}^2\theta_{\rm sph}\psi_s(\theta) && \text{Model I}\\ &= N_0{}^2\theta_{\rm cyl}H(x) = N_0{}^2\theta_{\rm cyl}\psi_c(\theta) && \text{Model II}\\ &= N_0{}^2 0.6\pi^{1/2}\theta_G \exp[-\theta^2/(0.6\,\theta_G)^2] && \text{Model III}\\ &= N_0{}^2 0.6\pi^{1/2}\theta_G\psi_e(\theta)\ ;\end{aligned} \tag{A.4}$$

where $x = 1 - 4\theta^2/\theta_c{}^2$ and the function $H(x) = 1$ for $x > 0$ and $H(x) = 0$ for $x < 0$. Since the main beam of the 140-foot antenna pattern has a very good circular symmetry, we can write the relation between maximum antenna temperature and brightness temperature in the form

$$T_{A_0} = \frac{\eta_B}{\Omega_m}\, 2\pi \int_0^\infty d\theta\,\theta f(\theta) T_b(\theta) \tag{A.5}$$

with

$f(\theta)$ for the antenna power pattern ,

$\Omega_m = 1.133\ \theta_A{}^2$ the main-beam solid angle ,

$\theta_A =$ the antenna HPBW ,

$\eta_B =$ the main-beam efficiency .

Substitution of equation (6) into equation (A.5) yields

$$\frac{2\pi}{\Omega_m}\int_0^\infty d\theta\,\theta f(\theta)\int N^2(\theta,\phi)\,d\phi = \frac{T_{A_0}}{82.35\,a\,\eta_B}\left(\frac{T_e}{^\circ\mathrm{K}}\right)^{0.35}\left(\frac{D}{\mathrm{kpc}}\right)^{-1.0}\left(\frac{\nu}{\mathrm{GHz}}\right)^{2.1}. \tag{A.6}$$

For the second integral on the left side we substitute equation (A.4). The functions $\psi(\theta)$ have the meaning of normalized brightness temperature distributions ($\psi_{\max} = 1$). With the notations defined by Baars *et al.* (1965*b*), we write for the source solid angle

$$\Omega_s = 2\pi\int_0^\infty d\theta\,\theta\psi(\theta) \tag{A.7a}$$

and for the modified source solid angle

$$\Omega'_s = 2\pi\int_0^\infty d\theta\,\theta\psi(\theta) f(\theta). \tag{A.7b}$$

Inserting the expressions (A.4) in equation (A.6) and using the relations (A.7a) and (A.7b), we obtain

$$\frac{T_{A_0}}{82.35\,a\,\eta_B}\frac{\Omega_m}{\Omega'_s}\left(\frac{T_e}{^\circ\mathrm{K}}\right)^{0.35}\left(\frac{D}{\mathrm{kpc}}\right)^{-1.0}\left(\frac{\nu}{\mathrm{GHz}}\right)^{2.1} = \begin{cases} N_0{}^2\theta_{\rm sph} & \text{Model I}\\ N_0{}^2\theta_{\rm cyl} & \text{Model II}\\ N_0{}^2 0.6\sqrt{(\pi)}\,\theta_G & \text{Model III}\ . \end{cases} \tag{A.8}$$

The flux density of a radio source is given by the expression

$$S_\nu = \frac{2kT_{A_0}}{A}\frac{\Omega_s}{\Omega'} = \frac{2kT_{A_0}}{\lambda^2\eta_B}\frac{\Omega_m\Omega_s}{\Omega'_s}, \tag{A.9}$$

© American Astronomical Society • Provided by the NASA Astrophysics Data System

1967ApJ...147..471M

where the relation $A = \eta_R \lambda^2/\Omega = \eta_B \lambda^2/\Omega_m$ is used. The source solid angles are computed by inserting the distribution functions equations (A.3) (I, 3) in the integral equation (A.7a)

$$\begin{aligned} \Omega_s &= \frac{\pi}{6}\,\theta^2_{\rm sph} && \text{Model I} \\ &= \frac{\pi}{4}\,\theta^2_{\rm cyl} && \text{Model II} \\ &= 1.133\,\theta_G{}^2 && \text{Model III}\,. \end{aligned} \tag{A.10}$$

Substitution of equations (A.9) and (A.10) in equation (A.8) yields

$$\frac{S_\nu \lambda^2}{82.35\,a\,2k}\left(\frac{T_e}{^\circ\mathrm{K}}\right)^{0.35}\left(\frac{D}{\mathrm{kpc}}\right)^{-1.0}\left(\frac{\nu}{\mathrm{GHz}}\right)^{2.1} = N_0{}^2 \begin{cases} \frac{\pi}{6}\,\theta^3_{\rm sph} & \text{Model I} \\ \frac{\pi}{4}\,\theta^3_{\rm cyl} & \text{Model II} \\ 1.133(0.6\sqrt{\pi})\,\theta_G{}^3 & \text{Model III}\,. \end{cases} \tag{A.11}$$

This equation would allow us to compute the electron density for the three models if we knew their apparent diameters. The apparent source HPW's as listed in Table 3 have been derived assuming a Gaussian brightness temperature distribution of the source. This is true, however, only for Model III; for Models I and II we have to compute the relation between the apparent diameters $\theta_{\rm sph}$ and $\theta_{\rm cyl}$, respectively, and their equivalent Gaussian HPW. This leads to

$$\theta_{\rm sph} = 1.471\,\theta_G \quad \text{and} \quad \theta_{\rm cyl} = 1.201\,\theta_G\,. \tag{A.12}$$

Substituting these relations in equation (A.11), we finally obtain for the average electron density of an H II region

$$\begin{aligned} \left(\frac{N_0}{\mathrm{cm}^{-3}}\right) = u_1 a^{1/2} 6.351 \times 10^2 &\left(\frac{T_e}{10^4\,^\circ\mathrm{K}}\right)^{0.175}\left(\frac{\nu}{\mathrm{GHz}}\right)^{0.05} \\ &\times\left(\frac{S_\nu}{\mathrm{f.u.}}\right)^{0.5}\left(\frac{D}{\mathrm{kpc}}\right)^{-0.5}\left(\frac{\theta_G}{\mathrm{min\,arc}}\right)^{-1.5}. \end{aligned} \tag{A.13}$$

The total mass of ionized hydrogen is then obtained by integrating the density distribution of the three models and multiplying the integrals with the mass of a hydrogen atom $m_{\rm H} = 1.67333 \times 10^{-24}$ g:

$$M = m_{\rm H}\int_v N(x,y,r)\,dV = m_{\rm H} D^3 2\pi \int d\theta\,\theta \int d\phi\, N(\theta,\phi)\,.$$

Substitution here of the density distributions (A.3), using the relations (A.12) and dividing M by the solar mass $M_\odot$, yields

$$\frac{M}{M_\odot} = u_2 a^{1/2} 0.3864 \left(\frac{T_e}{10^4\,^\circ\mathrm{K}}\right)^{0.175}\left(\frac{\nu}{\mathrm{GHz}}\right)^{0.05}\left(\frac{S_\nu}{\mathrm{f.u.}}\right)^{0.5}\left(\frac{D}{\mathrm{kpc}}\right)^{2.5}\left(\frac{\theta_G}{\mathrm{min\,arc}}\right)^{1.5}. \tag{A.14}$$

The numerical values of the factors u_1 and u_2 depend on the particular model chosen for the density distribution of the H II region. They are compiled in Table 4.

© American Astronomical Society • Provided by the NASA Astrophysics Data System

1967ApJ...147..471M

REFERENCES

Altenhoff, W., Mezger, P. G , Wendker, H and Westerhout, G 1960, *Veröff. Sternwärte, Bonn,* No 59, 48.
Baars, J. W. M., and Mezger, P. G. 1966, *Sky and Telescope,* **31,** 7
Baars, J. W M., Mezger, P. G., and Wendker, H. 1965*a*, *Z. f Ap* , **61,** 134.
———. 1965*b*, *Ap J* , **142,** 122
Bolton, J G , Gardner, F F. and Mackey, M. B. 1964, *Australian J Phys* , **17,** 340
Broten, N. W , Cooper, B F. C , Gardner, F F , Minnett, H C , Price, R. M , Tonking, F. G , and Yabsley, D. E 1965, *Australian J. Phys.*, **18,** 85
Howard, W E., III, and Maran, S P. 1965, *Ap. J Suppl* , **10,** 1.
Mezger, P. G , and Höglund, B 1967, *Ap. J.*, **147,** 490.
Oster, L 1961, *Rev. Mod Phys* , **33,** 525.
Small, M. 1965, *Sky and Telescope,* **30,** No 5
Wendker, H. 1966, *Mitt Ast. Inst Münster,* No. 10
Westerhout, G. 1958, *B A.N.*, **14,** 215.

© American Astronomical Society • Provided by the NASA Astrophysics Data System